J. Synchrotron Rad. (1997). **4**, 83–94

Time-Resolved X-ray Powder Diffraction Using a Large-Area CCD-Based Detector and Rietveld Refinement: Solid-State Polymerization of S_2N_2 to $(SN)_x$

S. O. Svensson, J. Birch, H. Müller and Å. Kvick*

ESRF, BP 220, 38043 Grenoble CEDEX, France. E-mail: kvick@esrf.fr

(*Received 30 July 1996; accepted 7 January 1997*)

A kinetic study of the solid-state polymerization of disulfur dinitride (S_2N_2) to polysulfur nitride [$(SN)_x$] has been performed, combining monochromatic high-energy (λ = 0.3263 Å) synchrotron radiation X-ray powder diffraction, a large-area (ø = 220 mm) CCD-based X-ray image-intensifier detector and Rietveld refinement. Recently developed techniques for detector calibration and reduction of two-dimensional images to one-dimensional diffraction patterns have been employed for data processing/analysis. Good fits were obtained after Rietveld refinement [R_p = 8.4%, wR_p = 9.4%, $\sin(\theta_{max})/\lambda$ = 0.585 Å^{-1}] of diffraction patterns of S_2N_2 from images with 2 s exposure time. The solid-state polymerization of S_2N_2 to $(SN)_x$ was followed at a maximum rate of two diffraction images per minute. Scale factors and cell parameters for S_2N_2 and β-$(SN)_x$ as functions of time were readily obtained after Rietveld refinement of the diffraction patterns obtained from each individual image throughout the polymerization. The polymerization was preceded by a lattice distortion of S_2N_2, and at 50% conversion the a axis had decreased by about 1% and the c axis had increased about 1%. The polymerization yielded not only the expected polymer β-$(SN)_x$, but also a small amount of a compound that could be another phase of $(SN)_x$.

Keywords: time-resolved studies; powder diffraction; Rietveld refinement; X-ray area detectors; charge-coupled device detectors; S_2N_2.

1. Introduction

The new third-generation synchrotron radiation sources, such as the European Synchrotron Radiation Facility (ESRF) in Grenoble, have opened up new areas for time-resolved X-ray diffraction experiments. The high flux of well collimated X-ray photons combined with fast-readout large-area X-ray detectors make time-resolved experiments feasible with time ranges as low as picoseconds (Bourgeois *et al.*, 1996). In this article we describe a time-resolved study on a molecular scale of a solid-state polymerization with a time resolution of two diffraction patterns per minute.

X-ray powder diffraction is a powerful tool for time-resolved *in situ* studies of phase transitions and solid-state reactions. Synchrotron radiation facilities offer the choice of energy-dispersive (white-beam) powder diffraction, or angular-dispersive (monochromatic) powder diffraction. Energy-dispersive powder diffraction is well suited for time-resolved studies; however, monochromatic powder diffraction offers better d-space resolution, which is important in multi-phase studies. Monochromatic powder diffraction has been used successfully in a large number of studies using either conventional sources (see, for instance, Bénard & Louër, 1995; Oyama, Hasegawa & Takei, 1994; Suda, Yashima, Kakihana & Yoshimura, 1994; Weber & Schweda, 1995) or synchrotron radiation (Pennartz, Löchner, Fuess & Wroblewski 1992; Christensen, Norby & Hanson, 1995; Rizzo, Doyle & Wroblewski, 1995; Christensen, Norby, Hanson & Shimida, 1996). These studies have either employed conventional θ–2θ scans or one-dimensional position-sensitive detectors. A two-dimensional position-sensitive detector (area detector) offers a number of advantages over the conventional θ–2θ scan and one-dimensional position-sensitive detectors in powder diffraction:

(*a*) The exposure time can be very short. This is also true for a one-dimensional position-sensitive detector; however, given the same exposure time and 2θ range, area detectors offer better signal to noise ratios.

(*b*) If the sample is not a perfect powder (*e.g.* with preferred orientation and/or large grain size) the diffraction patterns, obtained with a 2θ scan or with a one-dimensional position-sensitive detector, will contain systematic errors. In subsequent data analysis (*e.g.* Rietveld refinement) corrections must be applied to compensate for these errors, which can be a non-trivial task. With an area detector, these systematic errors can be minimized by integration around the Debye–Scherrer rings (averages out preferred orientations and spots from large grains) and/or masking of strong spots (*e.g.* from sample holders or large grain sizes). In fact, the two-dimensional powder diffraction image can be used to extract qualitative information on preferred orientation (Wright, Nelmes, Belmonte & McMahon, 1996).

X-ray area detectors have been combined with synchrotron radiation powder diffraction; however, this has mainly been in high-pressure studies (Nelmes & McMahon, 1994, and references therein). For these experiments, exposure times are generally long (>> 1 min), hence imaging-plate detector systems are well suited, offering a large dynamic range combined with a large number of (angular) resolution elements and no build-up of noise as function of exposure time. Time-resolved studies have to date been restricted to kinetically very slow reactions due to read-out times of the order of minutes. Recently developed CCD (charge-coupled-device)-based X-ray area detectors have read-out times of the order of 1–10 s. They are therefore very suitable for time-resolved studies on this timescale, with the drawback of a smaller number of resolution elements compared with imaging-plate detectors.

We chose to study the solid-state polymerization of disulfur dinitride $S_2N_2 \rightarrow$ polysulfur nitride $(SN)_x$ as a model reaction. S_2N_2, a highly unstable compound, is known to polymerize spontaneously to $(SN)_x$. $(SN)_x$ is a unique compound in that it is both an intrinsic electrical conductor and the only polymer known to date that exhibits a superconducting transition ($T_c \simeq 0.3$ K; Greene, Street & Suter, 1975). The polymerization time at ambient temperature is relatively slow and ranges, depending on the crystallite size, from hours to days. $(SN)_x$ can form several phases. Only one of these structures has been solved (Cohen *et al.*, 1976); in this article we refer to this structure as β-$(SN)_x$. Baughman, Apgar, Chance, MacDiarmid & Garito (1977) reported cell parameters of a different phase of $(SN)_x$; however, the structure could not be elucidated. We refer to this structure as α-$(SN)_x$.

We report in this article the results from a pilot experiment in which we combined the high flux of X-ray photons produced by the ESRF, a large-area X-ray detector and Rietveld refinement. It deserves mentioning in this context that time-resolved X-ray powder diffraction studies with higher time resolution than in the present case have been performed, *e.g.* Pennartz *et al.* (1992) reported a time resolution better than 10 ms using a one-dimensional position-sensitive detector. In contrast to previous work the emphasis of this study was to take advantage of a newly developed CCD-based X-ray area detector for the quantitative analysis of a topochemical reaction. With high-quality data, Rietveld refinement (Rietveld, 1969) gives not only accurate scale factors and cell parameters for the different compounds in the reaction mixture, but also yields information on atomic coordinates and temperature factors. We give a short description of the calibration of the detector system, describe the time-resolved measurement and the data reduction, present results of the Rietveld refinements and finally discuss the results both in instrumental/methodological terms and briefly comment on the solid-state polymerization of S_2N_2 to $(SN)_x$. The chemical aspects of the results will be reported elsewhere (Müller, Svensson, Birch & Kvick, 1997).

2. X-ray image intensifier and its calibration

An X-ray image intensifier/CCD detector system has been developed at the ESRF (Moy, 1994). It is a modular, high-performance detector well suited for time-resolved experiments. We used the model 49425 HX from Thomson Tubes Electroniques, which is a 220 mm-diameter modified standard medical tube, where the aluminium input window has been replaced by a beryllium window. A Princeton Instruments CCD camera cooled to 228 K was optically coupled to the output phosphor screen of the X-ray image intensifier.

The geometry of the X-ray image intensifier (the input surface is almost spherical, curved away from the sample) introduces considerable spatial distortion into the recorded image, and inhomogeneities of the scintillator in the tube introduce non-uniformity of the response distortion. Therefore, in order to obtain accurate crystallographic information in terms of diffracted X-ray intensity and position, calibration of the spatial distortion and the non-uniformity of response is necessary. In this experiment we have applied the methods reported earlier (Hammersley, Svensson & Thompson, 1994; Hammersley *et al.*, 1995) to calibrate the detector and correct the diffraction images.

The calibration of the non-uniformity of response requires a large homogeneous field of X-rays, preferably at the same wavelength as the planned experiment. In this experiment we have used a new technique of calibrating the non-uniformity of response developed at the ESRF (Moy *et al.*, 1996). A doped lithium borate glass plate is placed at the sample position. When illuminated with a beam of X-rays whose energy is slightly above the *K*-absorption edge of the dopant, an almost homogeneously fluorescent radiation is emitted and the elastic scattering is strongly absorbed. The fluorescent radiation is used to record a flood-field image on the detector, which is later used to produce a flat-field image. We chose to perform the experiment at 38 keV in order to use a lithium borate glass plate doped with 10% barium.

3. Experiment

3.1. *Sample preparation*

S_2N_2 was prepared at the ESRF chemistry laboratory by pyrolysis of tetrasulfur tetranitride (S_4N_4) on silver wool according to a modified literature procedure (Goehring & Voigt, 1956). Details of apparatus and procedure will be published elsewhere (Müller *et al.*, 1997). Through the whole preparation utmost care was taken to avoid any exposure of S_2N_2 to (atmospheric) humidity in order to obtain a starting material of high purity. Using Schlenk techniques, S_2N_2 was transferred with permanent cooling (195 K, dry ice) to a glove-bag filled with dry high-purity nitrogen, then loaded into glass capillaries (ø = 0.8 mm), flame-sealed and stored in liquid nitrogen under exclusion of light. In view of the pronounced sensitivity of both S_2N_2 and $(SN)_x$ to moisture their analytical characterization by standard methods is difficult. IR spectra of S_2N_2 and

the resulting polymer were in accordance with literature data; X-ray diffraction, however, is certainly the method of choice to determine the purity and composition of these compounds.

The S_2N_2 in sealed capillaries turned out to be much more stable at ambient temperature than described in the literature (Cohen *et al.*, 1976). Therefore we used a halogen lamp to trigger the polymerization. The optimal lamp-to-sample distance was found to be 6 cm. Using this distance, the temperature was measured to be about 313 K at the sample position, and the reaction was accelerated to a time of total conversion of ~1 h. The approximate sample mass amounted to 1–2 mg S_2N_2 per capillary.

3.2. *Experimental set-up*

The experiment was performed at the Materials Science high-power wiggler beamline (ID 11) at the ESRF [*ESRF Beamline Handbook*, 1995; beamline optics are discussed by Krumrey, Kvick & Schwegle (1995) and by Susini, Baker, Krumrey, Schwegle & Kvick (1995)]. The monochromated X-ray beam was set to an energy of 38.00 keV. The X-ray beam was set to 0.5 × 0.5 mm^2 at the sample position, where we have calculated the polarization of the X-ray to be 0.99 in the horizontal plane. The flux at sample position was measured using a calibrated photodiode to be 2.6 × 10^{10} photons s^{-1}. The capillaries were mounted on a κ-diffractometer with a horizontal φ axis. The sample-to-detector distance was determined to be 238.5 mm using a standard sample. The X-ray image intensifier was mounted slightly off-center, which allowed us to record the strongest Debye–Scherrer diffraction rings entirely, and to reach 0.855 Å (d-space) resolution at the edge of the detector. The CCD produced images with 1242 × 1152 pixels. The optics of the CCD detector was operated with a maximal aperture of F = 3, which corresponds to a gain of about 50 CCD readout counts per 38 keV X-ray photon.

3.3. *Data collection*

We used two exposure times, 2 and 20 s, in order to increase the dynamic range of the detector. The 2 s exposure allowed us to collect the whole diffraction pattern within the dynamic range of the detector, while the 20 s exposure time was chosen to obtain a better signal-to-noise ratio for weak intensity reflections. The sample was rotated by 10° for the 2 s exposures (the maximum speed of rotation was 6° s^{-1}) and by 45° for the 20 s exposures. The two exposure times were alternated throughout the data collection (*i.e.* every

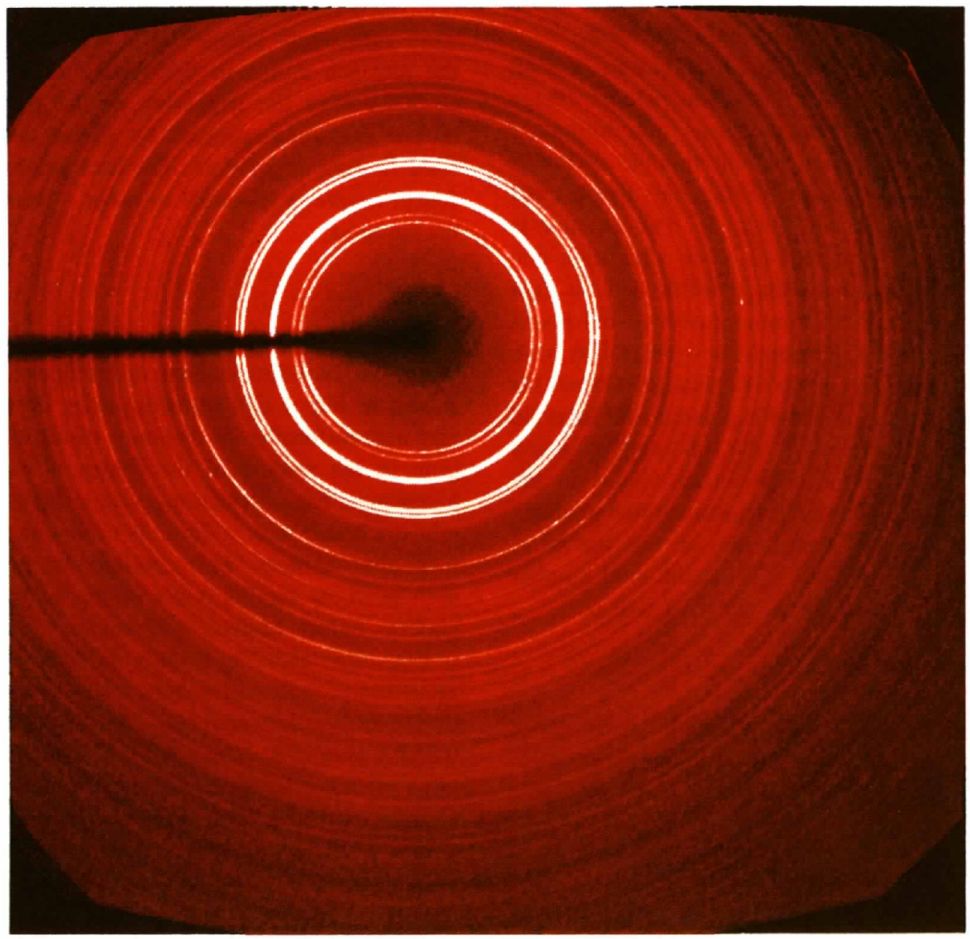

Figure 1
Diffraction image of S_2N_2 collected with an exposure time of 2 s, corrected for spatial- and non-uniformity of response distortion. The dark region in the middle of the image is the shadow of the beamstop. The irregular shape at the edge of the image is caused by the spatial distortion correction.

second image was exposed for 2 s and the others for 20 s). The read-out time plus data transfer to the hard disk was approximately 12 s, which allowed us to collect a sequence of two images with 2 and 20 s exposure time in less than a minute.

4. Data reduction and Rietveld analysis

The diffraction images were corrected for spatial distortion and non-uniformity of response distortion by the program *FIT2D* (Hammersley, 1995). The pixel size (freely adjustable, user input when calibrating the spatial distortion) was set to 120 × 120 μm. The corrected images were integrated with application of polarization and geometrical correction factors using the same program to give one-dimensional powder diffraction profiles corresponding to 2θ scans (Hammersley, Svensson, Hanfland, Fitch & Häusermann, 1996). The angular step of this pseudo-2θ scan was set to 0.01°, which for the chosen pixel size corresponds to an oversampling by a factor of three. For each angular bin, the number of pixels contributing to the intensity value of the bin was saved in order to estimate the inaccuracy due to photon statistics. The intensity values of the patterns were furthermore corrected for X-ray beam decay, and finally the background caused by the glass capillary was subtracted before Rietveld refinement.

The precision of intensity values in a pseudo-2θ scan produced after integration of a two-dimensional image cannot be estimated in the same manner as for a normal 2θ scan, the primary reason being that the number of pixels contributing to each angular bin in the one-dimensional diffraction profile increases with 2θ angle. The situation is furthermore complicated by pixel-to-pixel correlation due to the point-spread function of the detector and the fact that each 2θ bin is built up by summing over partial pixels (Hammersley *et al.*, 1996). However, it is crucial to have accurate estimates of the precision of the intensity values for least-squares refinement algorithms in general, and Rietveld refinement in particular. We chose the following approach to estimate the precision of the intensity values in the pseudo-2θ scans. For the 2θ bin i, let the integrated intensity be I_i, the number of pixels contributing to this bin be n_i and the gain of the detector be g. Then, the total number of photons $Ntot_i$ contributing to the 2θ bin i will be

$$Ntot_i = I_i n_i / g.$$

In the absence of pixel-to-pixel correlation, the estimated standard deviation due to (only) photon counting statistics is given by

$$\sigma(Ntot_i) = (I_i n_i / g)^{1/2}.$$

$\sigma(Ntot_i)$ must be divided by the number of pixels n_i in order to be normalized with respect to the intensity values I_i. $\sigma(Ntot_i)$ must furthermore be multiplied with the gain g (or, equally, the intensity values I_i could be divided by g). Finally, $\sigma(Ntot_i)$ is multiplied with a constant c, which is introduced in order to model the contribution of pixel-to-pixel correlations and detector noise:

$$\sigma(I_i) = \sigma(Ntot_i)(gc/n_i) = c(I_i g/n_i)^{1/2}.$$

We estimated the gain g of the detector to be about 50 (as mentioned above), and we chose the constant c to be 2. With these parameters we obtained reasonable values of the reduced χ^2 after refinement (see §5).

The diffraction patterns were refined with the Rietveld method using the program *GSAS* (Larson & Von Dreele, 1987). The polymerization product yielded diffraction peaks at low resolution ($2.5 < 2\theta < 4.2°$) which could be assigned neither to S_2N_2 nor to β-$(SN)_x$, and this 2θ region was therefore excluded from the refinement [the peaks could be assigned to α-$(SN)_x$, see discussion in §6.2]. One preferred orientation parameter was introduced (March–Dollase, direction [010], value 1.09, see discussion in §6.1). Scale factors for S_2N_2 and β-$(SN)_x$ were refined for all diffraction profiles. Cell parameters, three peak profile parameters (the pseudo-Voigt Gaussian profile width GW, the Lorentzian profile width LX and one asymmetry parameter) and the isotropic thermal parameters for the sulfur and the nitrogen atoms were refined when allowed (*i.e.* when the diffraction peaks of the corresponding phase were sufficiently intense). The positions of the sulfur and the nitrogen atoms in S_2N_2 were refined before and up to 500 s after the triggering of the polymerization. The atomic positions reported by Cohen *et al.* (1976) were used as starting positions. The background was refined as a fourth-degree polynomial in order to remove any residual background.

5. Results

A typical two-dimensional diffraction image of S_2N_2 is shown in Fig. 1 (2 s exposure time, corrected for spatial- and non-uniformity of response distortions). The dark region in the middle of the image is the shadow of the beamstop. The diffraction pattern after integration contained a broad peak at $2\theta \simeq 5°$ caused by diffuse scattering from the capillary. This capillary background (measured with an empty capillary) was subtracted from the diffraction patterns before Rietveld refinement.

Figs. 2(*a*) and 2(*b*) display diffraction patterns of S_2N_2 after background subtraction obtained with exposure times of 2 and 20 s, respectively. The resolution at $2\theta = 22°$ is 0.855 Å [$\sin(\theta)/\lambda$ =0.585 Å^{-1}]. In the same figures the patterns generated by the Rietveld refinement model are plotted together with the corresponding difference curves. The R values from the Rietveld refinement with 21 parameters refined are R_p = 8.4%, wR_p = 9.4% and reduced χ^2 = 1.73 for the 2 s exposure, and R_p = 6.7%, wR_p = 7.2% and χ^2 = 7.5 for the 20 s exposure. The refinement parameters for the two exposure times are summarized in Tables 1(*c*) and 1(*d*). As mentioned in §3.1, the best method of measuring the purity of S_2N_2 is X-ray diffraction. The scale factor of

β-$(SN)_x$ resulting from the refinement was below 10^{-4}. We take this, together with the good fit of the refined model, as evidence that the (crystalline) starting compound was S_2N_2 of high purity (>99.9%). The cell parameters and atomic coordinates (Tables 1*c* and 1*d*) differ slightly from those presented by Cohen *et al.* (1976) (Table 1*a*), which may be explained by the fact that, in their study, the S_2N_2 crystal was cooled to 140 K. The unit-cell parameters of β-$(SN)_x$ (Table 1*f*) agree with those presented by Cohen *et al.* (1976) (Table 1*b*) and by Heger, Klein, Pintschovius & Kahlert (1978). Bond distances and bond angles of S_2N_2 (Tables 1*c* and 1*d*) obtained after refinement of atomic positions are in agreement with those reported by Cohen *et al.* (1976).

A total of 100 images were collected from $t = -2000$ to $t = 6000$ s, where $t = 0$ is defined as the time when the light was switched on. The diffraction patterns as function of time from $t = 0$ to $t = 1500$ s are shown in Fig. 3. For clarity, only every second collected pattern (with 2 s exposure time) is plotted.

During the polymerization, spots appeared in the diffraction images. The spots were carefully removed by a mask before integration. The diffraction image at 65% conversion ($t = 830$ s) is presented in Fig. 4(*a*), the corresponding diffraction pattern and the difference curve after Rietveld refinement (14 parameters, $R_p = 11.2\%$, $wR_p = 15.1\%$, $\chi^2 = 2.9$, Table 1*e*) are displayed in Fig. 5(*a*). The diffraction

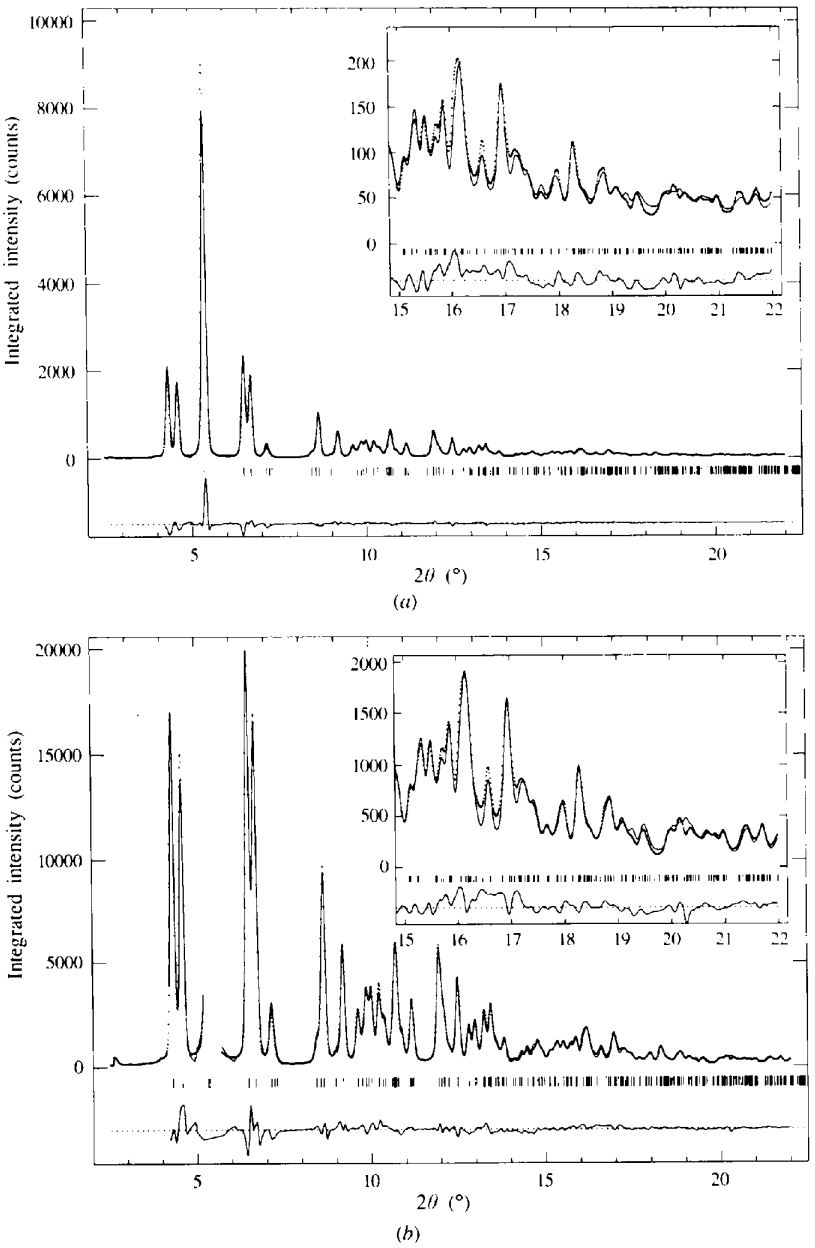

Figure 2
Result of Rietveld refinement of diffraction patterns of S_2N_2 before the polymerization, (*a*) 2 s exposure time and (*b*) 20 s exposure time. FWHM of the diffraction peaks is 0.13°. The region $2.5 < 2\theta < 4.7°$ has been removed from the Rietveld refinement because of the peaks in this region caused by the byproduct.

Table 1
Refinement parameters.

(*a*), (*b*) Structural values for S_2N_2 and β-$(SN)_x$ published by Cohen *et al.* (1976), obtained using single-crystal diffraction. The values for S_2N_2 were obtained at 143 K. (*c*) Rietveld refined parameters corresponding to the diffraction pattern shown in Fig. 2(*a*). (*d*) Rietveld refined parameters corresponding to the diffraction pattern shown in Fig. 2(*b*). (*e*) Rietveld refined parameters corresponding to the diffraction pattern shown in Fig. 5(*a*). Atomic coordinates were not refined. (*f*) Rietveld refined parameters corresponding to the diffraction pattern shown in Fig. 5(*b*). Atomic coordinates were not refined. (*g*) Structural parameters of β-$(SN)_x$ corresponding to Fig. 8(*b*). Observe that $\alpha < 90°$. Unit-cell parameters calculated with values from (*f*), atomic coordinates from Cohen *et al.* (1976) (*b*).

	(*a*)	(*b*)	(*c*)	(*d*)	(*e*)		(*f*)	(*g*)
Compound	S_2N_2	β-$(SN)_x$	S_2N_2	S_2N_2	S_2N_2	β-$(SN)_x$	β-$(SN)_x$	β-$(SN)_x$
Exposure time (s)	–	–	2	20	2		2	–
Structure	Monoclinic	Monoclinic	Monoclinic	Monoclinic	Monoclinic	Monoclinic	Monoclinic	Monoclinic
Space group	$P2_1/c$	$P2_1/c$	$P2_1/c$	$P2_1/c$	$P2_1/c$	$P2_1/c$	$P2_1/c$	$(P2_1/c)$*
a (Å)	4.485 (2)	4.153 (6)	4.517 (1)	4.518 (1)	4.475 (2)	4.162 (2)	4.144 (2)	4.429
b (Å)	3.767 (1)	4.439 (5)	3.845 (1)	3.845 (1)	3.855 (2)	4.431 (2)	4.429 (2)	4.144
c (Å)	8.452 (3)	7.637 (12)	8.496 (1)	8.495 (1)	8.535 (4)	7.664 (3)	7.668 (3)	7.407
β (°)	106.43 (3)	109.7 (1)	106.39 (1)	106.43 (1)	105.40 (8)	109.42 (3)	109.40 (2)	α = 77.55
S—N (Å)	1.657 (1)	1.593 (5)	1.647 (5)	1.659 (5)	–	–	–	–
	1.651 (1)	1.628 (7)	1.611 (5)	1.636 (4)	–	–	–	–
Angle S—N—S (°)	90.42 (6)	119.9 (4)	90.7 (3)	90.1 (3)	–	–	–	–
Angle N—S—N (°)	89.58 (6)	106.2 (2)	89.3 (3)	89.9 (3)	–	–	–	–
Sulfur								
x	0.20243 (8)	0.1790 (8)	0.1996 (4)	0.1994 (3)	–	–	–	0.2127
y	0.1210 (1)	0.7873 (6)	0.1107 (6)	0.1166 (4)	–	–	–	0.0847
z	0.10635 (4)	0.3443 (4)	0.1055 (2)	0.1054 (2)	–	–	–	0.0943
U_{iso}	–	–	0.056 (1)	0.043 (1)	–	–	0.039 (2)	–
Nitrogen								
x	–0.1735 (3)	0.141 (3)	–0.174 (1)	–0.175 (1)	–	–	–	0.568
y	0.0475 (4)	0.431 (2)	0.0520 (12)	0.0496 (8)	–	–	–	0.069
z	0.0778 (2)	0.322 (2)	0.0725 (5)	0.0751 (3)	–	–	–	0.072
U_{iso}	–	–	0.051 (2)	0.043 (1)	–	–	0.022 (3)	–
GW	–	–	20.3 (5)	21.1 (5)	–	–	24 (4)	–
LX	–	–	3.2 (2)	4.1 (2)	–	–	15 (1)	–
Asym	–	–	0.001 (2)	0.07 (2)	–	–	0.13 (7)	–
No. of parameters	–	–	21	21	15		15	–
No. of data points	–	–	1779	1728	1779		1779	–
R_p	–	–	0.084	0.067	0.112		0.1129	–
wR_p	–	–	0.094	0.078	0.151		0.155	–
Reduced χ^2	–	–	1.73	7.5	2.89		5.8	–

* Symmetry operators are (x, y, z), $(x + 1/2, -y, -z)$, $(-x, -y + 1/2, -z + 1/2)$, $(-x + 1/2, y + 1/2, z + 1/2)$.

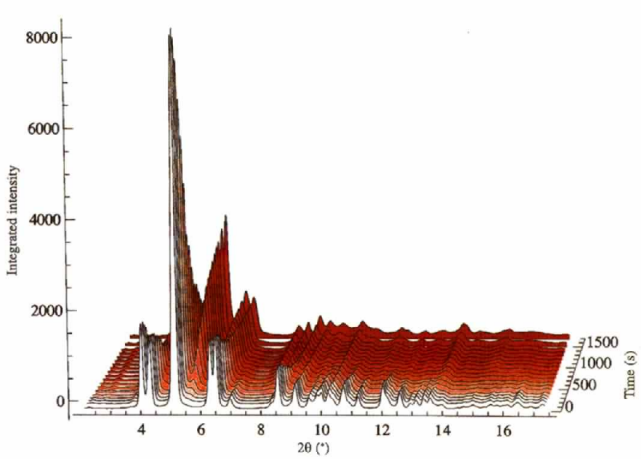

Figure 3
Diffraction patterns as function of time throughout the polymerization of S_2N_2 to β-$(SN)_x$. For clarity, only every second pattern with an exposure time of 2 s is plotted.

image of the end product [which mainly consists of β-$(SN)_x$] and the difference curve after Rietveld refinement (15 parameters, R_p = 11.3%, wR_p = 15.5%, χ^2 = 5.8, Table 1*e*) are shown in Figs. 4(*b*) and 5(*b*), respectively.

The weight percentages of S_2N_2 and β-$(SN)_x$ are plotted as function of time in Fig. 6(*a*). (+) refer to the 2 s exposures, and (◇) to the 20 s exposures. The scale factors in Fig. 6(*a*) have been normalized to set the scale factor of S_2N_2 to 100% for t = 0. It is evident from Fig. 6(*a*) that the two different exposure times give two different scale factors for S_2N_2 and β-$(SN)_x$ for $t < 0$ and $t > 1000$ s. This is due to the fact that, for these time periods, the strongest peak of the 20 s exposure had to be removed due to saturation before Rietveld refinement. The intensity of the byproduct α-$(SN)_x$ is plotted as function of time in Fig. 6(*b*). It is impossible to calculate the weight percent for α-$(SN)_x$ since its structure is unknown. Therefore we plot the time evolution of the peak intensity of the strongest reflection at 2θ = 3.9°.

Fig. 7 shows the cell parameters (Figs. 7*a*–7*d*) and the cell volume (Fig. 7*e*) of S_2N_2 as function of time. The unit cell of S_2N_2 starts to change as function of time before the polymerization is triggered by the lamp. After switching on the lamp ($t > 0$) the change of unit-cell parameters is strongly accelerated. However, this change of unit cell is not accompanied by changes of the unit-cell volume of S_2N_2. All curves in Fig. 7 show a discontinuity of about 0.1% at $t = 0$, which we attribute to thermal expansion of the S_2N_2 crystal caused by heating, see discussion in §6.1. For $t > 500$ s the S_2N_2 peaks vanish and hence the uncertainty rapidly increases.

The results of refinement of atomic coordinates of S_2N_2 during the polymerization are presented in §6.2. The Rietveld refinements yielded many other parameters as a function of time, but a full description of the results is beyond the scope of this article.

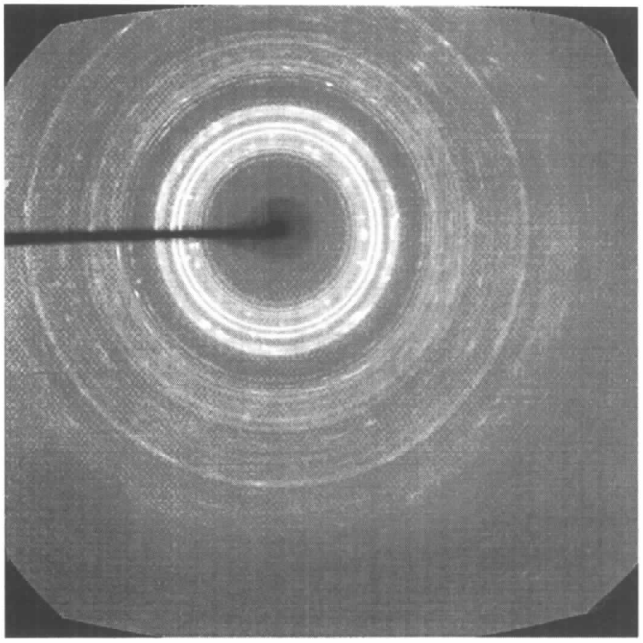

(*a*)

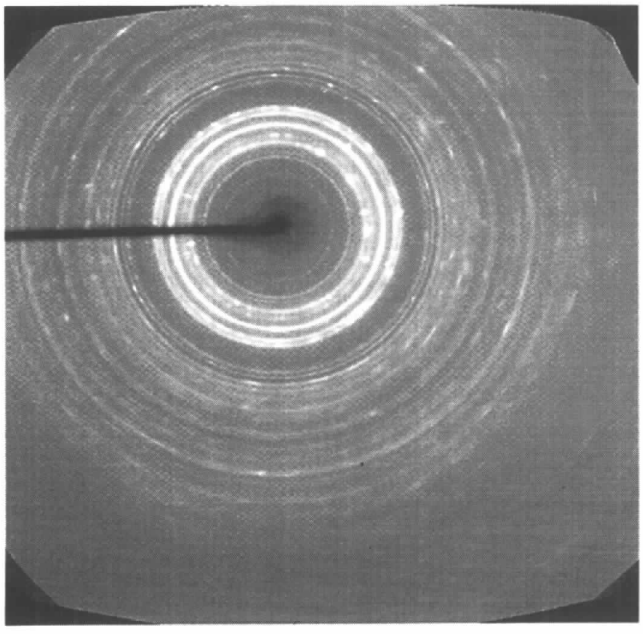

(*b*)

Figure 4
Diffraction images at 65% conversion (*a*) and of the end product (*b*).

6. Discussion

The discussion is divided into two parts. The first part discusses the pure instrumental or methodological aspects of the experiment, and the second part contains a brief discussion of the results in terms of the solid-state polymerization of S_2N_2 to $(SN)_x$.

6.1. *Instrument and measurement*

In order to compare our method with standard powder diffraction techniques, such as a θ–2θ scan or a one-dimensional position-sensitive detector, it is important to know the contribution of instrumental broadening to the width of the diffraction peaks. To estimate the instrumental broadening we simulated a distorted Debye–Scherrer diffraction ring one pixel wide (120 µm) convoluted with a point-spread function of 300 µm full width at half maximum (FWHM), which was measured on this detector system in an earlier study (Bourgeois, Moy, Svensson & Kvick, 1994). After correction of spatial distortion and integration the FWHM of the peak was 0.10°. The instrumental broadening is thus estimated to be 0.10° FWHM. The diffraction profiles of S_2N_2 in Fig. 2 have FWHMs of about 0.13°. Assuming Gaussian peak shapes, the peak width of the sample is calculated by quadratic subtraction to be 0.09°. Hence, for this experiment, the contributions to the width of the diffraction peaks are almost equally distributed between the instrument and the sample.

A striking result is the similarity of diffraction patterns, even at the highest angular resolution, for exposure times of 2 and 20 s (shown in Figs. 2*a* and 2*b*). Since the powder diffraction rings at high angular resolution of the 2 s exposure images are only ~10–100 counts above the background, one would expect this region in the one-dimensional integrated diffraction pattern to be considerably noisier compared with the same region in the diffraction pattern obtained from an image with ten times longer exposure. The similarity between the two diffraction patterns can be explained by the fact that the number of pixels from the diffraction image contributing to each angle in the one-dimensional pattern is high, *i.e.* even if the absolute intensity per input pixel is low, the total intensity per angle in the one-dimensional pattern can be high. Furthermore, the larger number of pixels contributing to peaks at higher 2θ makes high-resolution data not less accurate, even if the exposure time is the same as for the low-angle data (as is the case when collecting powder patterns with a θ–2θ scan or a one-dimensional position-sensitive detector).

The diffraction patterns 'suffer' from preferred orientation, mainly because the sample oscillation range was limited to 10° for the 2 s exposure (maximum speed of the rotation stage was 6° s^{-1}) and 45° for the 20 s exposure during data collection. Therefore one preferred orientation axis was introduced in the refinement. The axis and the value were refined for one pattern using the atomic positions reported by Cohen *et al.* (1976), and were kept constant during the refinement of all patterns. Minor differences between the measured and calculated diffraction profiles (difference curves in Figs. 2*a* and 2*b*) are obvious. We believe that these differences are caused mainly by residual (non-modelled) preferred orientation in the sample.

The Rietveld refinement of diffraction patterns obtained in the middle and at the end of the polymerization fit less well, as shown in Figs. 5(*a*) and 5(*b*). The images became more and more spotty, which is most probably due to an increase of crystallite size. However, the spotty images prove the strength of using area detectors in powder diffraction: a conventional θ–2θ scan or a one-dimensional position-sensitive detector would have produced diffraction patterns very hard to interpret. Indeed, when the images were first integrated without masking, the diffraction patterns yielded considerably poorer fits after refinement. We therefore believe that it is justified to remove the spots with masks, even though they are produced by the sample, because of the limited rotation of the φ axis during exposure. If the axis could have been rotated continuously at high speed, the images would probably not have required any masking. Another possible reason for the less good fits is the fact that,

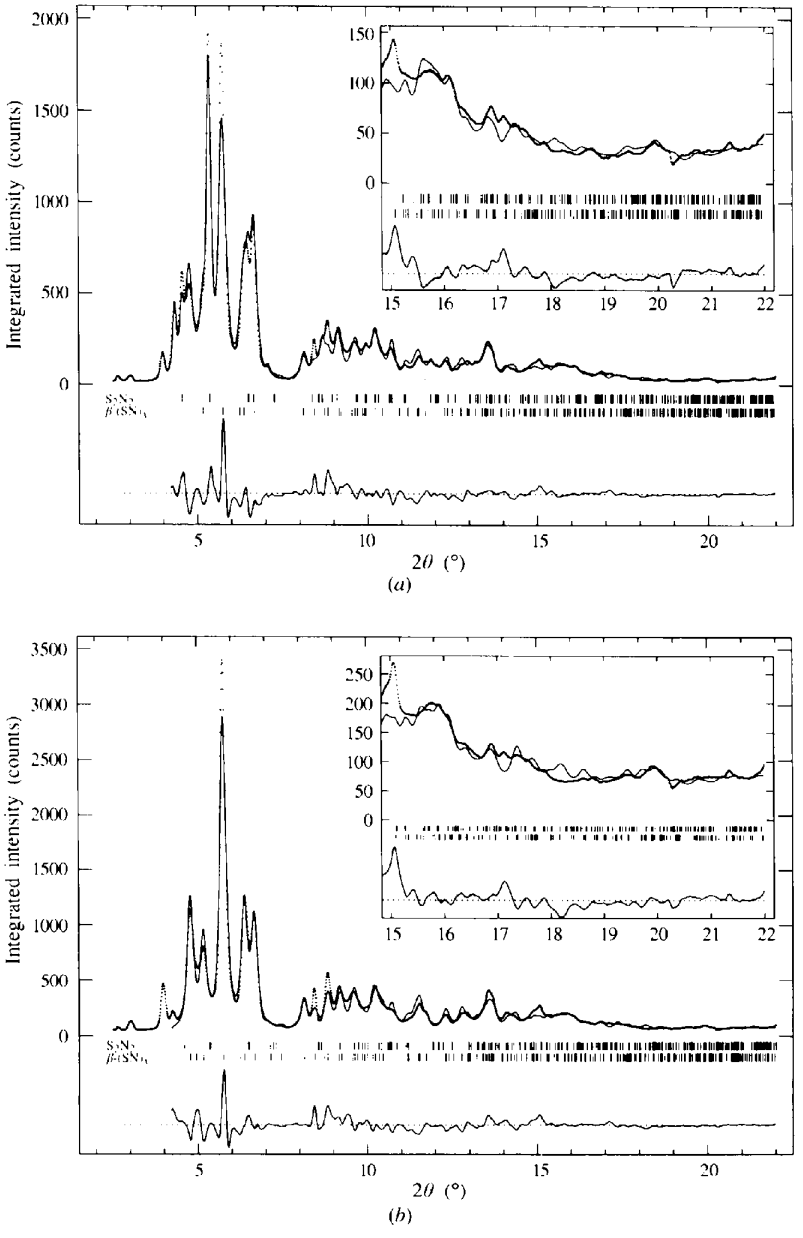

Figure 5
Result of Rietveld refinement at 65% conversion (*a*) and of the end product (*b*) (corresponding diffraction patterns to the images in Fig. 4).

apart from α-$(SN)_x$, other unknown crystalline phases may exist in the end product (Rickert, Ishida, Lando, Koenig & Baer, 1980).

The scale factors refined from diffraction patterns with 20 s exposure are higher for $t < 0$ than those from 2 s exposure, and lower for $t > 1000$ s (Fig. 6*a*). The reason for this discrepancy is unclear; however, detector non-linearity can be excluded by earlier characterizations of the detector system (Moy & Gibney, 1992). We believe that the most reliable scale factor is the scale factor from the 20 s exposure patterns, since these patterns suffer less from preferred orientation.

We attribute the discontinuity of the cell parameters at $t = 0$ to a thermal expansion of the unit cell. The discontinuity could, in principle, also have been caused by a change of the electromagnetical environment (*i.e* switching on the light) of the X-ray image intensifier, which is extremely sensitive to such changes. We rule out this possibility for a number of reasons: (*a*) The centre of the diffraction patterns do not change for images taken with $t < 0$ and $t > 0$. A change of the spatial distortion which conserves the centre of the diffraction rings is very unlikely. (*b*) No distortion of the circular shape of the diffraction rings for $t > 0$ could be found. (*c*) The shift in unit-cell parameters is non-isotropic.

We used two exposure times (2 and 20 s) in order to increase the dynamic range of the CCD detector; however, the very similar results after Rietveld refinements of patterns with the two exposure times makes us confident that we could have performed the whole experiment with only 2 s exposures if more caution had been taken to avoid preferred orientation. Therefore it may be concluded that the time resolution can be substantially increased by the use of faster readout CCDs, currently being developed at the ESRF with a readout time of 0.1 s (Labiche, Segura-Puchades, van Brussel & Moy, 1996).

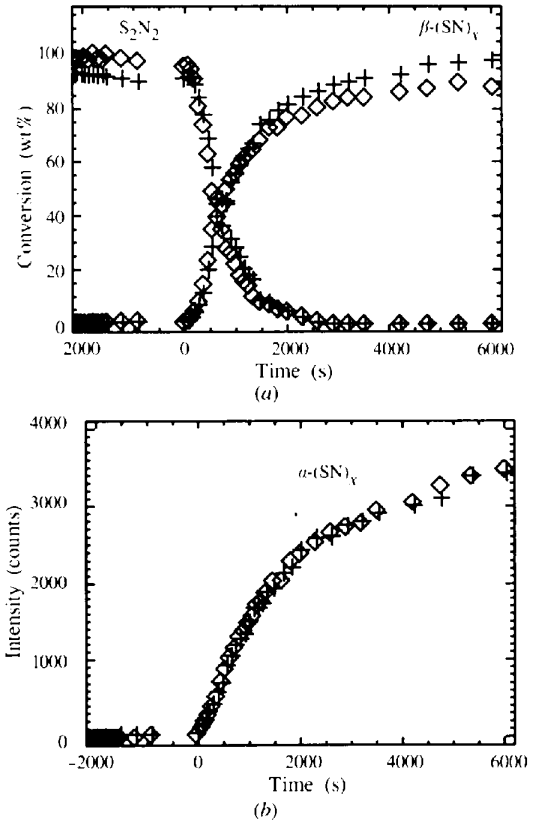

Figure 6
Scale factors as function of time (*a*) S_2N_2 and β-$(SN)_x$, and (*b*) byproduct. (+) refer to the 2 s exposures, and (◇) to the 20 s exposures.

6.2. *Polymerization of S_2N_2 to $(SN)_x$*

We shall here highlight a few aspects of the title reaction in order to illustrate the potential of the method for kinetic studies of solid-state reactions and phase transitions. A more detailed discussion, however, is beyond the scope of this article and will be given elsewhere (Müller *et al.*, 1997).

The conversion *versus* time curves (displayed in Fig. 6) for the starting compound S_2N_2 and the formation of $(SN)_x$ are approximately inversely proportional to each other. The sigmoidal shape of these curves resembles those of autocatalytic reactions and qualitatively matches earlier results reported by Kanazawa, Stejny & Keller (1992), although the time resolution of our experiment was much higher.

The crystal structures of S_2N_2 and β-$(SN)_x$ are shown in Fig. 8. The S_2N_2 molecules (Fig. 8*a*) consist of two sulfur and two nitrogen atoms forming almost perfect squares, which are situated on symmetry centres in the S_2N_2 crystal. The β-$(SN)_x$ crystal (Fig. 8*b*) is presented in a rather unorthodox choice of unit cell (monoclinic cell with $\alpha < 90°$, Table 1*g*) in order to visualize more clearly the relation between the crystal structures of S_2N_2 and β-$(SN)_x$. It is evident from Fig. 8 that, during the polymerization process, the unit cell of S_2N_2 must undergo a dramatic distortion when forming $(SN)_x$.

Our measurements show that the polymerization of S_2N_2 is preceded by a lattice distortion. After triggering of the reaction this lattice distortion is accelerated, and at *ca* 50% conversion the *a* axis has decreased by about 1% and the *c* axis has increased about 1% (Fig. 7). The origin of this lattice distortion *must* originate in a spatial rearrangement on a molecular level of the reactant. However, the refinement of atomic positions is, compared with the refinement of unit-cell parameters, less reliable. The refinement of atomic position of S_2N_2 in the initial step of the reaction ($0 < t < 500$ s, 50% conversion) could therefore not yield information on changes in bond lengths and angles with the same accuracy as the unit-cell parameters. No geometrical change of the S_2N_2 molecules larger than 1% was found.

Surprisingly, we found that the title reaction yielded not only the expected polymer β-$(SN)_x$ but also a byproduct identified by three diffraction peaks at low resolution, which could neither be assigned to S_2N_2 nor to β-$(SN)_x$. We first assigned the three diffraction peaks to S_4N_4 (Lucia & Coppens, 1978), but a simulation of the peaks of S_4N_4 with the experimental peak width revealed a poor fit (see

Fig. 9). A simulation of the three lowest order peaks of α-$(SN)_x$ (a = 6.251, b = 4.429, c = 4.807 Å, $\alpha = \beta = \gamma$ = 90°) gave a better agreement (Fig. 9). The d spacings corresponding to the three reflections are 6.200, 4.709 and 4.412 Å. Baughmann *et al.* (1977) suggested the space group $P2_12_12_1$ for α-$(SN)_x$. However, if the symmetry of α-$(SN)_x$ is orthorhombic, the space group for α-$(SN)_x$ cannot have higher symmetry than $P222$ since these reflections would otherwise be forbidden by symmetry.

7. Conclusions

We have presented a time-resolved measurement, combining synchrotron radiation X-ray powder diffraction, a large-area two-dimensional X-ray detector (an X-ray image intensifier optically coupled to a CCD camera) and Rietveld refinement, of the solid-state polymerization of S_2N_2 to $(SN)_x$. The high flux of X-rays, combined with the integration of two-dimensional images to one-dimensional diffraction patterns, allowed us to obtain good fits after Rietveld refinement from diffraction patterns with exposure times of 2 s. The time resolution was not flux limited but limited by the read-out time of the CCD (12 s). Using future fast-readout CCDs time resolutions better than 1 s should be feasible.

The instrumental peak broadening was calculated to be 0.10°. The most important factor contributing to this width was the detector point-spread function. Thus, the X-ray image intensifier/CCD detector system used is a compromise between large area, readout time and angular resolution, that however offers data-acquisition times orders of magnitude faster than a θ–2θ scan of comparable range and angular resolution, and with higher angular/energy resolution than X-ray energy-dispersive powder diffraction.

The polymerization of S_2N_2 was preceded by a lattice distortion. At 50% conversion, the a axis had decreased by about 1% and the c axis had increased about 1%. However, no geometrical change of the S_2N_2 molecules was found larger than 1%. The polymerization was found to yield not only the expected polymer β-$(SN)_x$, but also a small amount of a compound which could be α-$(SN)_x$.

The authors would like to thank Andy Fitch, Jenny Noreng, Christine Jouan and Sanna Karhu for help with the tedious preparation of S_2N_2, Anette Frost Jensen and Heinz Graafsma for assistance in the measurements, Jean-

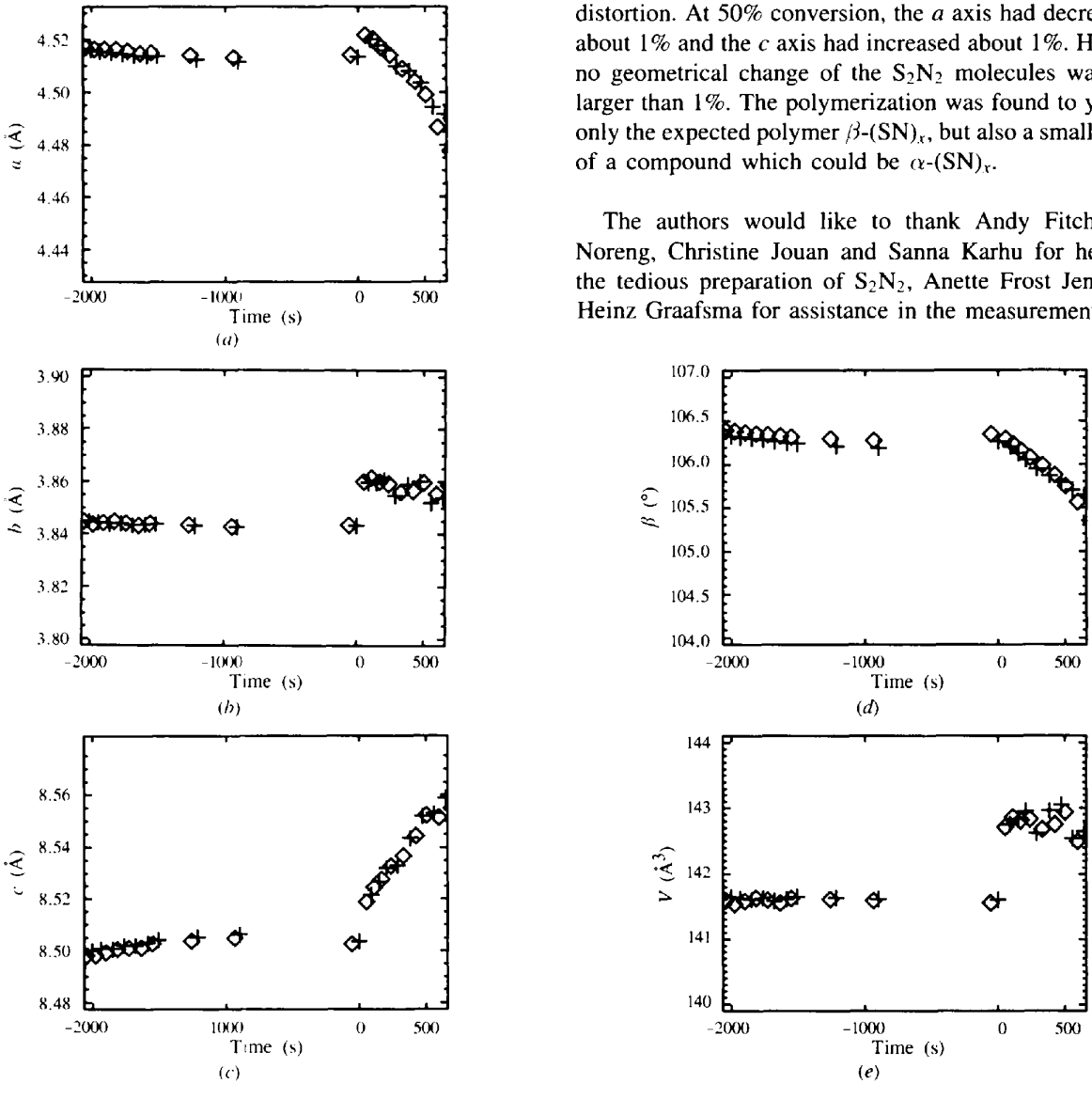

Figure 7
Cell parameters of S_2N_2 (*a*) a axis, (*b*) b axis and (*c*) c axis, (*d*) β angle and (*e*) cell volume. The discontinuity at t = 0 is due to thermal expansion of the S_2N_2 unit cell after raising the temperature from 293 to 313 K.

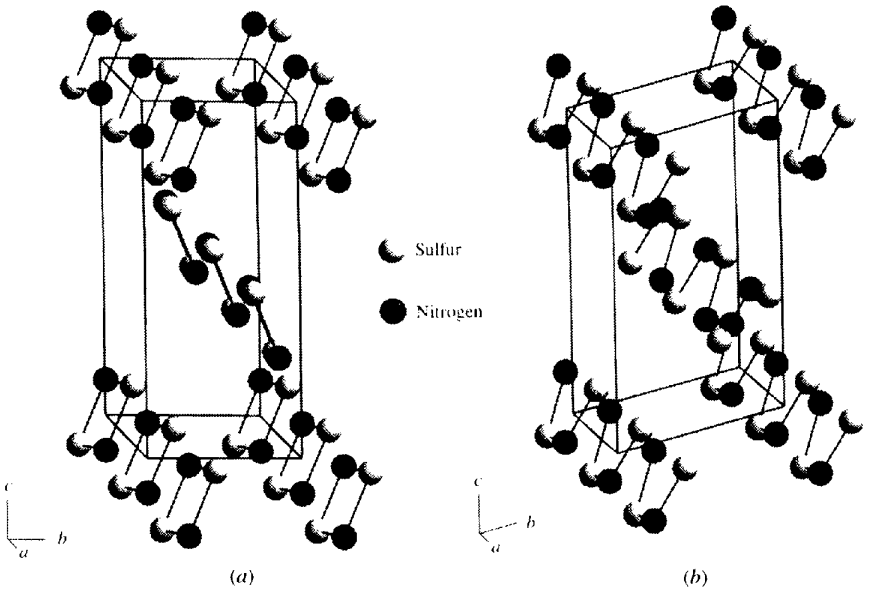

Figure 8
Crystal structure of (*a*) S_2N_2 (*b*) β-$(SN)_x$.

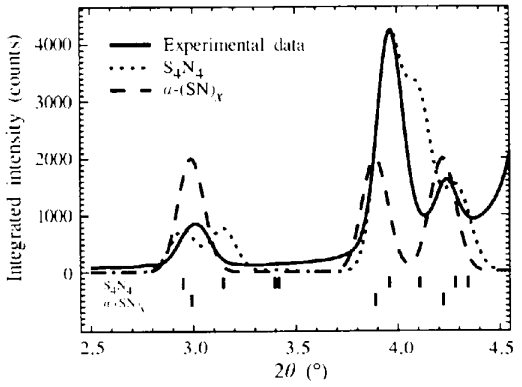

Figure 9
Diffraction peaks caused by the byproduct together with simulated peaks for S_4N_4 and α-$(SN)_x$.

Pierre Moy for assistance with the detector, and Dominique Bourgeois for the calculation of the polarization.

References

Baughman, R. H., Apgar, P. A., Chance, R. R., MacDiarmid, A. G. & Garito, A. F. (1977). *J. Chem. Phys.* **66**, 401–409.

Bénard, P. & Louër, D. (1995). *J. Phys. Chem. Solids*, **56**(10), 1345–1352.

Bourgeois, D., Moy, J. P., Svensson, S. O. & Kvick, Å. (1994). *J. Appl. Cryst.* **27**, 868–877.

Bourgeois, D., Ursby, T., Wullf, M., Pradervand, C., Legrand, A., Schildkamp, W., Labouré, S., Srajer, V., Teng, T. Y., Roth, M. & Moffat, K. (1996). *J. Synchrotron Rad.* **3**, 65–74.

Christensen, A. N., Norby, P. & Hanson, J. C. (1995). *J. Solid State Chem.* **114**, 556–559.

Christensen, A. N., Norby, P., Hanson, J. C. & Shimida, S. (1996). *J. Appl. Cryst.* **29**, 265–269.

Cohen, M. J., Garito, A. F., Heeger, A. J., MacDiarmid, A. G., Mikulski, C. M., Saran, M. S. & Kleppinger, J. (1976). *J. Am. Chem. Soc.* **98**(13), 3844–3848.

ESRF Beamline Handbook (1995). ESRF, Grenoble, France.

Goehring, M. & Voigt, D. (1956). *Z. Anorg. Allg. Chem.* **256**, 181–190.

Greene, R. L., Street, G. B. & Suter, L. J. (1975). *Phys. Rev. Lett.* **34**, 577–579.

Hammersley, A. P. (1995). *FIT2D Reference Manual*. Internal Report EXP/AH/95-01. ESRF, Grenoble, France.

Hammersley, A. P., Svensson, S. O., Hanfland, M., Fitch, A. N. & Häusermann, D. (1996). *High Pressure Res.* **14**, 235–248.

Hammersley, A. P., Svensson, S. O. & Thompson, A. (1994). *Nucl. Instrum. Methods*, **A346**, 312–321.

Hammersley, A. P., Svensson, S. O., Thompson, A., Graafsma, H., Kvick, Å. & Moy, J. P. (1995). *Rev. Sci. Instrum.* **66**, 2729–2733.

Heger, G., Klein, S., Pintschovius, L. & Kahlert, H. (1978). *J. Solid State Chem.* **23**, 341–347.

Kanazawa, H., Stejny, J. & Keller, A. (1990). *J. Mater. Sci.* **25**, 3838–3842.

Krumrey, M., Kvick, Å. & Schwegle, W. (1995). *Rev. Sci. Instrum.* **66**, 1715–1717.

Labiche, J. C., Segura-Puchades, J., van Brussel, D. & Moy, J. P. (1996). *ESRF Newsl.* **25**, 41–43.

Larson, A. C. & Von Dreele, R. B. (1987). Laboratory Report LA-UR-86-748. Los Alamos Laboratory, USA.

Lucia, M. L. & Coppens, P. (1978). *Inorg. Chem.* **17**, 2336–2338.

Moy, J. P. (1994). *Nucl. Instrum. Methods* **A348**, 641–644.

Moy, J. P. & Gibney, S. (1992). Internal Report EXP/JPM/SG/92/21. ESRF, Grenoble, France.

Moy, J. P., Hammersley, A. P., Svensson, S. O., Thompson, A., Brown, K., Claustre, L., Gonzalez, A. & McSweeney, S. (1996). *J. Synchrotron Rad.* **3**, 1–5.

Müller, H., Svensson, S. O., Birch, J. & Kvick, Å. (1997). *Inorg. Chem.* In the press.

Nelmes, R. J. & McMahon, M. I. (1994). *J. Synchrotron Rad.* **1**, 69–73.

Oyama, Y., Hasegawa, M. & Takei, H. (1994). *Jpn. J. Appl. Phys.* **33**, 4779–4781.

Pennartz, P. U., Löchner, U., Fuess, H. & Wroblewski, T. (1992). *J. Appl. Cryst.* **25**, 571–577.

Rickert, S. E., Ishida, H., Lando, J. B., Koenig, J. L. & Baer, E. (1980). *J. Appl. Phys.* **51**(10), 5194–5200.

Rietveld, H. M. (1969). *J. Appl. Cryst.* **2**, 65–71.

Rizzo, F., Doyle, S. & Wroblewski, T. (1995). *Nucl. Instrum. Methods*, **B97**, 479–482.

Suda, H., Yashima, M., Kakihana, M. & Yoshimura, M. (1994). *J. Phys. Chem.* **99**, 6752–6754.
Susini, J., Baker, R., Krumrey, M., Schwegle, W. & Kvick, Å. (1995). *Rev. Sci. Instrum.* **66**, 2048–2052.
Weber, W. & Schweda, E. (1995). *Z. Anorg. Allg. Chem.* **621**, 617–623.
Wright, N. G., Nelmes, R. J., Belmonte, S. A. & McMahon, M. I. (1996). *J. Synchrotron Rad.* **3**, 112–119.